IASS 2020/21 SURREY 7
International Conference on Spatial Structures 2020/21

Proceedings of the IASS Annual Symposium 2020/21 and the 7th International Conference on Spatial Structures
Inspiring the Next Generation
23 – 27 August 2021, Guildford, UK
S.A. Behnejad, G.A.R. Parke and O.A. Samavati (eds.)

A discrete topology optimisation method with feature size control for partial double-layer gridshell design

Yongpeng HE*[, a], Paul SHEPHERD[a], Jie WANG[a]

*[, a] Department of Architecture and Civil Engineering, University of Bath, Bath, UK. BA2 7AY
yh2173@bath.ac.uk

Abstract

A density-based topology optimisation method for discrete structures with minimum and maximum feature size control of solid phase is proposed in this paper. The feature size of solid phase is defined as the radius of the minimal circumscribed circle of solid elements. The minimum feature size is achieved by density filtering and Heaviside projection while the maximum feature size is enforced by limiting the local material amount. Firstly, the proposed method is tested on a planar structure to demonstrate the successful control on minimum and maximum feature size of solid phase, as well as to reveal the effect of parameters. Then, the method is applied to a single-layer gridshell to identify the optimal material distribution under the uniformly distributed load. Based on the optimisation results of the single-layer gridshell, second-layer grids are added to form partial double-layer gridshells. Linear static analysis is carried out to investigate the mechanical properties of the obtained gridshells. Results show that, under the external load, the stress and displacement distributions within the whole structures are rather uniform, except for the support regions and the mid-span areas between the neighbouring supports.

Keywords: topology optimisation, discrete structure, minimum feature size, maximum feature size, partial double-layer gridshell, second-layer grid addition.

1. Introduction

Topology optimisation can identify the optimal material distribution within a given design domain and has been applied widely in structural design. So far, topology optimisation of discrete structures (also termed discrete topology optimisation) is usually carried out on a ground structure which consists of candidate elements formed by interconnecting nodes in the design domain (Dorn *et al.* [4]). For application to large-span structures or for obtainment of high-resolution structural layouts, the ground structure is usually required to have dense nodal distribution and a high level of interconnected potential members. The use of dense ground structures might lead to complicated optimisation results, which can have a large number of short members, narrow-spaced or crossed-over members and hair-like features (members with small cross-sectional areas). To reduce the complexity, Parkes [13] proposed the "joint cost" function to penalise the short members, Kanno and Fujita [11] imposed an upper bound constraint on the number of nodes in the structures, Fairclough and Gilbert [5] limited the angles between adjacent members and prohibited simultaneous presence of crossed-over members, Ramos and Paulino [14] proposed a high-pass filter to remove the members with small cross-sectional areas during the optimisation process. Additionally, He and Gilbert [10] proposed geometry optimisation as a post-processing step to rationalise the results.

This paper addresses the complexity of discrete topology optimisation results by imposing feature size control on the structural elements. The feature size is defined as the radius of the minimal circumscribed circle of same-phase (present or removed) elements. As shown in Figure 1, same-phase elements are

lumped together, the black lines represent elements that are present (solid elements), while the grey lines represent elements that have been removed (void elements). The red circle is the minimum circumscribed circle for that group of solid elements and the radius of this circle is termed the feature size of the solid phase, while the radius of the blue dash-dotted circle represents the feature size of the void phase. The complexity of the structural layout is controlled by enforcing the feature size of the solid phase to be larger than the specified minimum value and smaller than the maximum threshold.

The discrete topology optimisation problem is formulated within the framework of the SIMP (Solid Isotropic Material with Penalisation) approach (Sigmund [15]) and is solved based on a ground structure with low-level connectivity. The design variables are attached to the pseudo densities of elements in the ground structure and are constrained within the range of [0, 1], with 0 representing void elements and 1 for solid elements. The minimum feature size control of the solid phase is achieved by a cone-shape filter, which essentially is a convolution operator that averages the element density with its neighbours. This cone-shape filter was proposed for sensitivity filtering by Sigmund [16] to resolve the issues of checkerboard patterns and mesh-dependency, as well as to achieve minimum feature size control in topology optimisation of continuum structure (also termed continuum topology optimisation). The smearing effect of the cone-shape filter leads to more elements having intermediate densities. To drive the element density toward extreme values (0 or 1), a projection scheme based on the Heaviside step function was proposed by Guest *et al.* [8]. This projection scheme is adopted in this paper to facilitate the binary design and minimum feature size control in discrete topology optimisation. To control the maximum feature size of the solid phase, a local material constraint (Guest [9]) limiting the amount of material that can be present within a certain region of each element is implemented. By incorporating the filtering and projection schemes, the solid elements in the structural layout cluster towards a feature size larger than the user-specified minimum. Furthermore, the feature size is restricted to be less than the prescribed upper bound by the element-wise local material constraints.

To demonstrate the efficiency on feature size control and to reveal the effect of parameters, first the proposed method is tested on a planar cantilever beam. Then, the method is applied on a single-layer gridshell structure. The optimisation results of the gridshell structure are used further to guide the second-layer grid additions in partial double-layer gridshell design. Gridshell structures can embrace freeform geometry and provide long-span unobstructed inner space. However, they are also vulnerable in stability and stiffness owing to their intrinsic shallow structural depth. To enhance their mechanical properties, second-layer grids can be added into the single-layer structures to form partial double-layer gridshells. Investigations on formation and mechanical performance of partial double-layer gridshells can be found in Chen *et al.* [3], Li *et al.* [12] and Tian *et al.* [20]. However, existing literature is mostly focused on regular-shaped gridshells, such as the spherical or cylindrical domes, within which the second-layer grids are configured along the circumferential/radial or transversa/longitudinal directions. To explore the optimal partial double-layer gridshell design, the results generated by the proposed discrete topology optimisation method are taken as a representation of the optimal material distribution and therefore are used to guide the second-layer grid additions.

The remainder of this paper is organised as follows. Section 2 gives the introduction of the filtering and projection schemes, the local material constraint as well as the optimisation procedure. Section 3 presents the optimisation results of the 2D cantilever beam and the hexagonal-shaped single-layer gridshell. Based on the optimisation results of the gridshell, second-layer grids are added to form partial double-layer gridshells. The formation and mechanical analysis results of the gridshells are presented in Section 4. Finally, the conclusion of this paper and the potential extensions of the proposed method are given in Section 5.

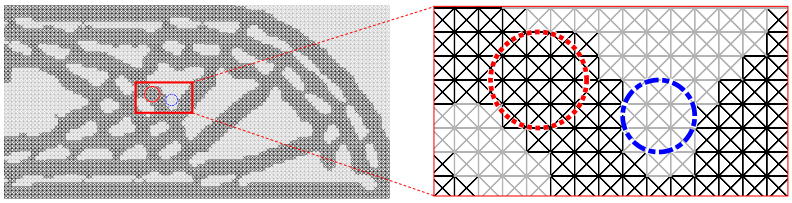

Figure 1: Illustration of feature sizes of solid and void phases (Black lines: elements with densities of 1; gray lines: elements with densities of 0; red circle: feature size of solid phase; blue dash-dotted circle: feature size of void phase)

2. Topology optimisation of discrete structure

The discrete topology optimisation problem is formulated within the framework of the SIMP approach (Sigmund [15]), with pseudo densities ρ of elements being the design variables ($\rho \in [0, 1]$). To achieve minimum feature size control of the solid phase, a filtering scheme modifying the current element density by taking into account its neighbouring elements is adopted. It is preferable that the optimisation result displays clear structural layout, formed by purely solid or void (ρ=0 or 1) elements. To tackle the smeared effect on element density caused by the filter, a smooth Heaviside step function is applied to project the intermediate densities towards 0 or 1. To control the maximum feature size of the solid phase, a local material constraint restricting the maximum amount of material that can be present within the specified region of each element is implemented. In this section, introduction of the filtering and projection schemes, the local material constraint is presented, followed by the optimisation procedure.

2.1. Filtering

Filtering schemes have been widely adopted in density-based continuum topology optimisation to resolve the issues of checkerboard pattern and mesh-dependency due to their easy implementation and prominent effectiveness. The cone-shaped filter was initially applied to modify element sensitivity (Sigmund [16]), later it was used as a density filter (Boudin [2]). For a comprehensive review of variants of filter in continuum topology optimisation, the reader is referred to Sigmund [17].

The cone-shaped filter is adopted here to convert the design variables from design field to filtered field. The filtered density is defined as the sum of weighted densities of elements within the filter zone. The filter zone for an individual element is defined as:

$$\boldsymbol{N}_{e,\min} = \{i \mid \|\boldsymbol{x}_i - \boldsymbol{x}_e\|_2 \leq R_{\min}\} \tag{1}$$

where $\boldsymbol{x}_e$ is the centroid (mid-point) of the considered element, and $\boldsymbol{x}_i$ is the centroid of the element in the filter zone, $R_{\min}>0$ is the filter radius. $\|\ \ \|_2$ returns Euclidean length of the vector.

The filtered density can be expressed as:

$$\tilde{\rho}_e = \frac{\sum_i^{\boldsymbol{N}_{e,\min}} \rho_i v_i w_i}{\sum_i^{\boldsymbol{N}_{e,\min}} v_i w_i} \tag{2}$$

where $\rho_i \in [0, 1]$ is the pseudo density of element, and is the design variable. $\tilde{\rho}_e$ is the filtered density. v_i is the volume of element, which is equal to $A_i L_i$ (section area×element length). w_i is the weighting factor, which decays linearly with the increase of elements' centroid-to-centroid distance, that is:

$$w_i = R_{\min} - (\|\boldsymbol{x}_i - \boldsymbol{x}_e\|_2) \tag{3}$$

The differential of the filtered density with respect to the design variable is:

$$\frac{\partial \tilde{\rho}_e}{\partial \rho_i} = \frac{v_i w_i}{\sum_i^{\boldsymbol{N}_{e,\min}} v_i w_i} \tag{4}$$

2.2. Projection

The filtering scheme acts as a weighted average operator, which drags down the high density and pulls up the low density, and therefore leads to more elements with intermediate densities. A smooth Heaviside function based on the exponential function was applied in Guest *et al.* [8]. It projects the densities larger than a threshold towards 1 and reduce densities less than the threshold towards 0, to facilitate the desired binary design. Herein, a tanh-based Heaviside function (Wang *et al.* [21]) is implemented, the projected density is expressed as:

$$\bar{\tilde{\rho}}_e = \frac{\tanh(\beta\eta) + \tanh(\beta(\tilde{\rho}_e - \eta))}{\tanh(\beta\eta) + \tanh(\beta(1-\eta))} \tag{5}$$

where $\eta \in [0, 1]$ is the prescribed threshold, chosen as 0.5 for this paper. β is the parameter that controls the sharpness of projection, the larger the β, the more rigorous the projection. In this paper, β is gradually increased from 1 to 128 as iterations progress.

The differential of the projected density with respect to the filtered density is:

$$\frac{\partial \bar{\tilde{\rho}}_e}{\partial \tilde{\rho}_e} = \frac{\beta(1 - \tanh^2(\beta(\tilde{\rho}_e - \eta)))}{\tanh(\beta\eta) + \tanh(\beta(1-\eta))} \tag{6}$$

2.3. Local material constraint

The principle of the local material constraint is to limit the maximum amount of solid material that can be present in the checking zones (Guest [9]). The checking zone is defined as a ring-shaped area centred at the considered element (Fernández *et al.* [6]):

$$\boldsymbol{N}_{e,\max} = \{i \mid R_{\min} < \|x_i - x_e\|_2 \leq R_{\max}\} \tag{7}$$

where $\boldsymbol{x}_e$ is the centroid of the considered element, and $\boldsymbol{x}_i$ is the centroid of the element in the checking zone, $R_{\min}$ is the filter radius. $R_{\max}$ is the outer radius for the checking zone, corresponding to the maximum feature size of solid phase. $\| \ \|_2$ returns Euclidean length of the vector.

To assure the feature size of solid phase smaller than $R_{\max}$, the sum of material in the checking zone is restricted to be a portion of the full local material, the local material constraint is formulated as:

$$s_e = \frac{\sum_i^{\boldsymbol{N}_{e,\max}} \bar{\tilde{\rho}}_i v_i}{\sum_i^{\boldsymbol{N}_{e,\max}} v_i} \leq \varepsilon_{\max} \tag{8}$$

where $\varepsilon_{\max}<1$ is the upper bound for the local material fraction and is set to 0.8 in this paper.

The differential of the local material constraint with respect to the projected density is:

$$\frac{\partial s_e}{\partial \bar{\tilde{\rho}}_i} = \frac{v_i}{\sum_i^{\boldsymbol{N}_{e,\max}} v_i} \tag{9}$$

By following the approach in Fernández *et al.* [6], A *p*-norm aggregation function is adopted to convert the element-wise local material constraints into a single constraint function, the aggregated constraint function can be expressed as:

$$P = \left(\frac{1}{n}\sum_{e=1}^{n} {s_e}^q\right)^{\frac{1}{q}} \leq \varepsilon_{\max} \tag{10}$$

where s_e is the element-wise local material constraint, q is the aggregation factor, n is the number of elements in the ground structure.

The differential of the aggregated function with respect to the element-wise constraint is derived as:

$$\frac{\partial P}{\partial s_e} = \left(\frac{1}{n}\sum_{e=1}^{n} {s_e}^q\right)^{\frac{1}{q}-1} \frac{1}{n} {s_e}^{q-1} \tag{11}$$

By applying the Chain Rule, the differential of the aggregated constraint function with respect to the design variable is expressed as:

$$\frac{\partial P}{\partial \rho_e} = \sum_{i}^{\boldsymbol{N}_{e,\min}} \left(\sum_{j}^{\boldsymbol{N}_{i,\max}} \frac{\partial P}{\partial s_j} \frac{\partial s_j}{\partial \bar{\tilde{\rho}}_i}\right) \frac{\partial \bar{\tilde{\rho}}_i}{\partial \tilde{\rho}_i} \frac{\partial \tilde{\rho}_i}{\partial \rho_e} \tag{12}$$

where $\partial\tilde{\rho}_i/\partial\rho_e$, $\partial\bar{\tilde{\rho}}_i/\partial\tilde{\rho}_i$, $\partial s_j/\partial\bar{\tilde{\rho}}_i$ and $\partial P/\partial s_j$ can be calculated using Eqs. (4,6,9&11), respectively.

2.4. Optimisation procedure

The projected density $\bar{\tilde{\rho}}_e$ presented in Section 2.2 is used to interpolate the elemental material stiffness. Following the modified SIMP approach (Andreassen *et al.* [1]), the elemental material stiffness can be calculated as:

$$E(\bar{\tilde{\rho}}_e) = E_{\min} + (\bar{\tilde{\rho}}_e)^p (E_0 - E_{\min}) \tag{13}$$

where $E_{\min}$ is the material stiffness for void elements, and is set to a small value to avoid singularity of the structural stiffness matrix, which might occur if chain-like connections or isolated elements are present during the optimisation process. E_0 is the element material stiffness for solid elements, and p is the penalisation factor which, if larger than 1, will penalise the material stiffness of elements with intermediate densities.

The element stiffness matrix is calculated based on the interpolated material stiffness given by Eq. (13), and then the element stiffness matrix is assembled to form the structural stiffness matrix. The structural stiffness matrix can be expressed as:

$$\boldsymbol{K}(\bar{\tilde{\boldsymbol{\rho}}}) = \sum_{e} E(\bar{\tilde{\rho}}_e) \boldsymbol{k}_e^0 \tag{14}$$

where $\boldsymbol{k}_e{}^0$ represents the stiffness matrix for elements with unit material stiffness.

The compliance minimisation problem subject to global material volume constraint and the aggregated local material constraint is formulated as:

$$\begin{aligned} \min \quad & C(\boldsymbol{\rho}) = \boldsymbol{U}^{\mathrm{T}}\boldsymbol{K}\boldsymbol{U} = \sum_{e} E(\bar{\tilde{\rho}}_e) \boldsymbol{u}_e^{\mathrm{T}} \boldsymbol{k}_e^0 \boldsymbol{u}_e \\ \text{s.t.} \quad & \boldsymbol{K}(\bar{\tilde{\boldsymbol{\rho}}})\boldsymbol{U} - \boldsymbol{F} = \boldsymbol{0} \\ & g(\bar{\tilde{\boldsymbol{\rho}}}) = \textstyle\sum_e \bar{\tilde{\rho}}_e v_e \,/V^0 - \alpha \le 0 \\ & P = \left(\frac{1}{n}\sum_{e=1}^{n} {s_e}^q\right)^{\frac{1}{q}} \le \varepsilon_{\max S} \end{aligned} \tag{15}$$

where $\boldsymbol{\rho} = [\rho_1, \dots, \rho_e, \dots, \rho_n]$ is the vector of design variables, $\rho_e \in [0, 1]$ and n is the number of elements in the ground structure. $\boldsymbol{U}$ is the nodal displacement vector, $\boldsymbol{K}$ is the structural stiffness matrix, $\boldsymbol{F}$ is the nodal force vector. $\boldsymbol{u}_e$ is the element deformation, $g(\bar{\tilde{\boldsymbol{\rho}}})$ is the global material volume constraint function, V^0 is the material volume when all elements are solid ($\bar{\tilde{\boldsymbol{\rho}}} = \boldsymbol{1}$), $V^0 = \sum_e v_e$. α is the user-defined material volume fraction.

The sensitivity of the objective function to the design variable can be calculated using the Chain-rule:

$$\frac{\partial C}{\partial \rho_e} = \sum_{i}^{\boldsymbol{N}_{e,\min}} \frac{\partial C}{\partial \bar{\tilde{\rho}}_i} \frac{\partial \bar{\tilde{\rho}}_i}{\partial \tilde{\rho}_i} \frac{\partial \tilde{\rho}_i}{\partial \rho_e} \tag{16}$$

where expressions of $\partial\tilde{\rho}_i/\partial\rho_e$ and $\partial\bar{\tilde{\rho}}_i/\partial\tilde{\rho}_i$ are shown in Eqs. (4) and (6), respectively. $\partial C/\partial\bar{\tilde{\rho}}_i$ is the differential of the structural compliance with respect to the element projected density, which can be obtained by the adjoint method:

$$\frac{\partial C}{\partial\bar{\tilde{\rho}}_i} = [-p(E_0 - E_{min})(\bar{\tilde{\rho}}_i)^{p-1}\boldsymbol{u}_i^{\mathrm{T}}\boldsymbol{k}_i^0\boldsymbol{u}_i] \tag{17}$$

$\partial C/\partial\bar{\tilde{\rho}}_i$ is intuitively modified by pre-multiplying with element material stiffness $E(\bar{\tilde{\rho}}_i)$, which gives:

$$\frac{\partial C^*}{\partial\bar{\tilde{\rho}}_i} = E(\bar{\tilde{\rho}}_i)\frac{\partial C}{\partial\bar{\tilde{\rho}}_i} \tag{18}$$

It is worth noting that, the term $E(\bar{\tilde{\rho}}_i)$ in Eq. (18) brings about extra penalisation effect, it tends to drag down the sensitivity of the elements with intermediate densities, and will possibly modify the ordering of them, but it has no effect on the ordering of the sensitivity of the elements with densities of 0 or 1. Based on the numerical studies conducted by the authors, it was found that using $(\partial C/\partial\bar{\tilde{\rho}}_i)^*$ rather than $\partial C/\partial\bar{\tilde{\rho}}_i$ in Eq. (16) can facilitate the evolution of binary designs. Therefore, all of the results presented in this paper are obtained by using $(\partial C/\partial\bar{\tilde{\rho}}_i)^*$ instead of $\partial C/\partial\bar{\tilde{\rho}}_i$ when calculating Eq. (16).

Similar to Eq. (16), the sensitivity of the global material volume constrain function to the design variable can be expressed as:

$$\frac{\partial g}{\partial\rho_e} = \sum_i^{\boldsymbol{N}_{e,\min}} \frac{\partial \mathrm{g}}{\partial\bar{\tilde{\rho}}_i}\frac{\partial\bar{\tilde{\rho}}_i}{\partial\tilde{\rho}_i}\frac{\partial\tilde{\rho}_i}{\partial\rho_e} \tag{19}$$

where $\partial g/\partial\bar{\tilde{\rho}}_i = v_i/V^0$, $\partial\tilde{\rho}_i/\partial\rho_e$and $\partial\bar{\tilde{\rho}}_i/\partial\tilde{\rho}_i$ can be calculated by Eqs. (4) and (6).

The sensitivity of the aggregated local material constraint function to the design variable is shown in Eq. (12).

To solve the problem presented in Eq. (15), the sensitivity information obtained by Eqs. (12), (16) and (19) is made use of, and the Method of Moving Asymptotes (MMA) (Svanberg [19]) is adopted to update the design variables. To stabilise the convergence process, a continuation scheme for the penalisation factor p in the SIMP approach and the sharpness factor β in projection scheme is implemented (Fernández *et al.* [7]). The penalisation factor p for SIMP starts from 1, then increases by 1 every 50 iterations until it reaches a max of 3. The sharpness factor β starts from 1, then doubles every 50 iterations until it reaches 128 or the problem converges. The aggregation factor is q=100. The moving step for design variable updating in MMA is m=0.05. The pseudo code for solving the problem is shown as follows:

1. Define the design domain, input $R_{\min}$, $R_{\max}$, α.
2. Initialise the parameters, $\boldsymbol{\rho}=\boldsymbol{\alpha}$, p=1, $p_{\max}$=3, β=1, $\beta_{\max}$=128, $\varepsilon_{\max}$=0.8, q=100, m=0.05, *change*=1.
3. while *change*>0.01 and *iter*<1000
4. *iter*=*iter*+1;
5. Solve FE problem based on the projected density $\bar{\tilde{\boldsymbol{\rho}}}$;
6. Calculate the objective and constraint functions, as well as their sensitivities (Eqs. 12,16&19);
7. Update design variable to get $\boldsymbol{\rho}_{\text{new}}$ using MMA;
8. Calculate the *change* = $\|\boldsymbol{\rho}_{\text{new}} - \boldsymbol{\rho}\|_\infty$;
9. if mod(*iter*, 50)==0
   p = min{p+1, $p_{\max}$};
   β = min{2β, $\beta_{\max}$};
   end
10. end while.
11. Output the topology defined by the projected density $\bar{\tilde{\boldsymbol{\rho}}}$.

3. Numerical examples

To validate the effectiveness of the proposed method, the compliance minimization problems subject to global material volume constraint and with minimum and maximum size control, are solved based on a 2D cantilever beam and a hexagonal gridshell structure. The results for these two examples are presented in this section.

3.1. 2D cantilever beam

The dimensions, loading and boundary conditions, as well as the discretisation of the structure are shown in Figure 2. The design domain is discretised with 100×50 unit-length square cells. Based on the initial discretisation (the horizontal and vertical boundary elements of the square cells), the diagonal elements are generated by interconnecting the nodes of the square cells. Combining the horizontal, vertical and diagonal elements, the ground structure with level-one connectivity is formed, of which the full view and local amplification are shown in Figure 2b.

The 2D cantilever beam is optimised firstly with only minimum feature size control, then with both minimum and maximum feature size control. To simulate the structure, truss elements with a solid circular section are adopted, with radius of cross section set to 0.1 (1/10×length of base cell). The material volume fraction α is set to 0.6. The elasticity for solid material is E_0=1, and for void material is E_{min}=10^{-9}. A concentrated force (F=1) acting at right bottom corner of the design domain is considered. The sensitivities of the objective function and constraint functions are in different magnitude, leading to slow convergence when solving sub-problems in MMA. To bring the magnitude of sensitivities of constraint functions close to that of objective function, the constraint functions and their sensitivities are scaled up by 1000.

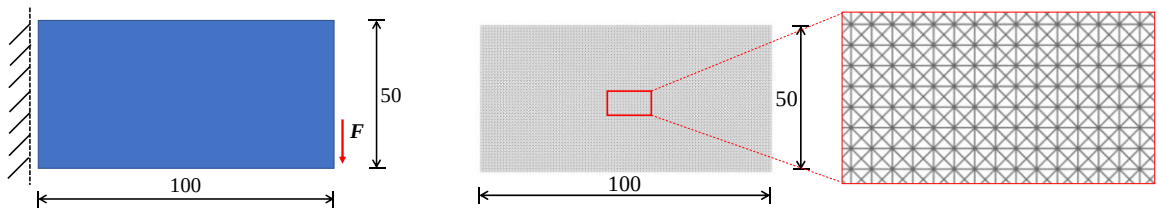

(a) Design domain and boundary conditions

(b) Structure discretisation

Figure 2: Design information of the 2D cantilever beam

3.1.1. Minimum size

In the proposed method, the minimum size control is realised by the filtering scheme, and it is expected that the minimum feature size of the solid phase in the optimal structural layout will equal the filter radius. To confirm this, the problem is solved firstly without filtering then with filtering, and with R_{min}=1, 2, respectively.

The optimisation results and the corresponding structural compliance (*Comp*) are presented in Figure 3, where Figure 3a shows the optimal topology for the case without filtering, and Figures 3b&c are the solutions for the cases with filtering. Without filtering, there is no control on the feature size and the connective relationship of the elements is totally determined by their mechanical contribution and material volume ratio. As shown in Figure 3a, the upper and lower parts of the cantilever beam, as well as the force-applied area have the most sophisticated connection and densest material distribution, implying the complexity of force transferring in these areas.

For the cases with filtering, the minimum feature size of the solid phase is increasing with the increase of R_{min}. The results generated with R_{min}=1 is shown in Figure 3b. By comparing the structural layout and the black-filled circle at the right top of the figure which indicates the desired feature size, it can be found that the solid elements have lumped to display a minimum feature size larger than R_{min}=1. Figure

3c shows the result for the case of R_{min}=2, in which the structural layout has displayed a minimum feature size close to R_{min}=2. As can be seen from Figure 3a&b&c, from the case without filtering to the case with filtering and with increased R_{min}, the connective relationship of the solid phase in the optimal layout is becoming less complicated, and this is because the filter acts as a density averaging operator and has filtered out the structural features.

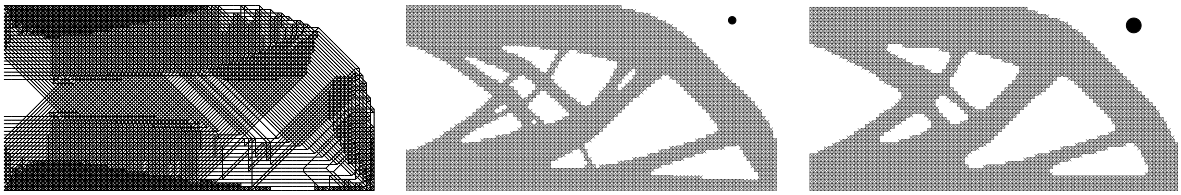

(a) Without filtering (b) R_{min}=1 (c) R_{min}=2

Figure 3: Optimisation results of the 2D cantilever beam with minimum feature size control (The black solid circle at right top symbolises the filter zone defined by R_{min})

3.1.2. Minimum and maximum size

In this section, problems with minimum and maximum feature size control are investigated. The minimum feature size is controlled by filtering & projection, and the maximum feature size is achieved by limiting the amount of material within the checking zone of each element.

The optimisation problems are solved with two different combinations of $\{R_{min}, R_{max}\}$, i.e., {1, 2} and {2, 3}. The results are presented in Figure 4. Figure 4a shows the result for the problem with {R_{min}=1, R_{max}=2}. The feature size of the solid phase has been controlled well, which is in general larger than R_{min}=1 but strictly less than R_{max}=2. Similarly, the feature size of the solid phase in the result corresponding to {R_{min}=2, R_{max}=3} is bounded by R_{min}=2 and R_{max}=3, as shown in Figure 4b. For these two cases, the solid elements have been distributed among the whole design domain and the separation between the solid phase is clear, facilitating the interpretation of the connective relationship of solid elements. Additionally, the results clearly indicate the sophisticated force-flowing paths for the cantilever beam.

Note that, the minimum feature size control of the solid phase achieved by the adopted filtering and projection schemes might not be strictly satisfied, as can be seen from Figure 4, where the feature size of the solid phase in some areas is less than the specified filter radius. This phenomenon has also been investigated in (Wang *et al.* [21]) within the framework of continuum topology optimisation. For a stricter control, reformulating the optimisation problem with robust formulation (Wang *et al.* [21] and Sigmund [18]) might be useful. Furthermore, there are some protruded solid elements (within the red dotted ellipse) near the right bottom of the design domain for the result corresponding to {R_{min}=2, R_{max}=3}, as shown in Figure 4b. The protruded elements start to occur at the late iterations, and they cannot further develop to reach the bottom possibly due to the high sharpness factor β in projection scheme and the high penalisation factor p, and also because of the small moving step for design variable updating. A smoother continuation scheme for p and β might be helpful to remedy this issue.

(a) R_{min}=1, R_{max}=2 (b) R_{min}=2, R_{max}=3

Figure 4: Optimisation results of the 2D cantilever beam with minimum and maximum feature size control (The black-filled circle at right top symbolises the filter zone defined by R_{min} while the red solid hollow circle represents the checking zone defined by R_{max} and the red dotted ellipse refers to the protruded elements)

3.2. Hexagonal gridshell

The design domain, ground structure and boundary condition of the hexagonal gridshell are shown in Figure 5. The gridshell has a height 20, its planar projection is a hexagon with edge length 60. The hexagonal shell can be generated by conducting trimming operations on a sphere of radius 100. Discretisation of the structure is carried out based on its planar projection firstly. On planar projection, the structure is discretised by equilateral triangles with an edge length of 1.5. Then, the planar discretisation is projected back to the surface to form the ground structure.

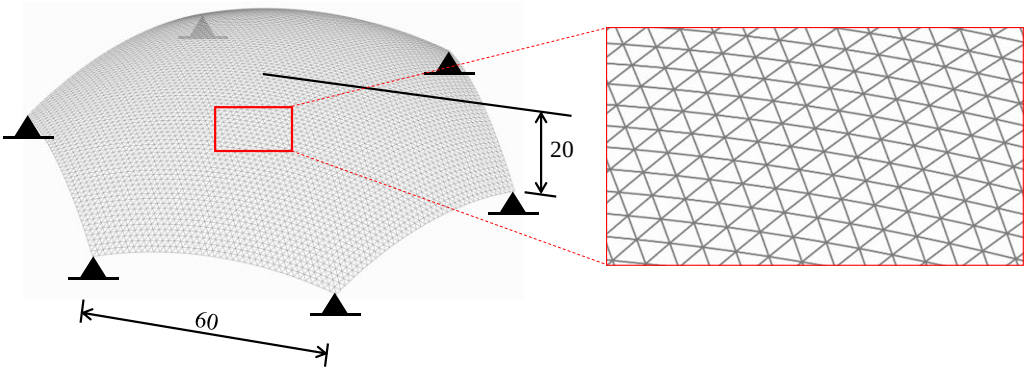

Figure 5: Design information of the hexagonal gridshell

A concentrated force with an amplitude of F=0.001 is applied at each node in the structure to simulate the uniformly distributed load. There are 4921 nodes in total and therefore the total applied load is 4.921. To avoid singularities during the optimisation process due to the distributed load, the structure is assumed to have two-layer of elements. The first layer is assigned with a fixed material stiffness of E_{top}=0.01. The second layer is used for optimisation and each element is assigned a pseudo density (design variable) indicating their status. The material elasticity for the second-layer element is E_0=1 if it is with density 1, E_{min}=10^{-9} if with density 0. For those elements with intermediate densities, their material stiffness is calculated through Eq. (7). The application of the top-layer elements is to avoid large displacements under the distributed load, therefore avoiding singularity in the sensitivity of structural compliance.

3D beam elements are adopted with a hollow circular section of outer diameter 0.15 and wall thickness 0.005. The Poisson's ratio is 0.3. The material volume fraction α is set to 0.6 and the problem is solved with both minimum and maximum feature size control, with parameter settings of $\{R_{min}, R_{max}\}$={2, 3} and {4, 5}. Similar to the 2D example, the constraint functions and their sensitivities are scaled up by an amplification factor of 1000.

The results of the topology optimisation problem with these two combinations of parameters $\{R_{min}, R_{max}\}$ are shown in Figure 6. Similar to the previous examples, in general the feature size of the solid phase in the optimal structure layout is constrained within the range of $[R_{min}, R_{max}]$. The structural layout corresponding to $\{R_{min}$=2, R_{max}=3$\}$ is more complicated than that of $\{R_{min}$=4, R_{max}=5$\}$, whilst the latter displays a feature size of the solid phase obviously larger than the former.

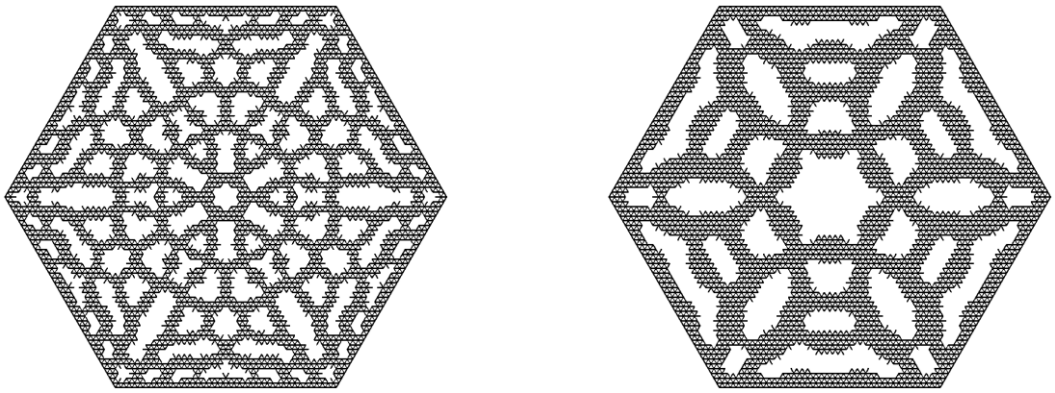

(a) R_{min}=2, R_{max}=3 (b) R_{min}=4, R_{max}=5

Figure 6: Optimisation results of the hexagonal gridshell with minimum and maximum feature size control

4. Design of partial double-layer gridshells

To enhance the mechanical properties of the single-layer gridshell, second-layer grids are added to form partial double-layer structures. The discrete topology optimisation results of the single-layer gridshell shown in Figure 6 indicate the optimal material distribution under the specified load, and therefore are used to guide second-layer grid addition. The second-layer grids are added based on the dual principle proposed by Conway *et al.* [22]. The nodes for second-layer structures (bottom nodes) are generated by offsetting the centroids of the triangular faces on top layer with an offsetting distance of 1.5. Then, the bottom nodes are connected to the vertexes of their affiliated faces to form web-members. The bottom chord members are generated based on the neighbouring relationship of the top faces, following the dual principle. Based on the structural layout shown in Figure 6a, second-layer grids are added, resulting into a partial double-layer gridshell (Gridshell-1). The generation process of Gridshell-1 is shown in Figure 7. To deal with the overhanging elements in the structural layout, extra elements (green lines in Figure 7a) are added to form closed triangular faces, as indicated by Figure 7a. The bottom chords are generated as a dual graph of the top faces and are shown in Figure 7b. The web-members are shown in Figure 7c and the whole structure of GridShell-1 is shown in Figure 7d. Based on the structural layout given in Figure 6b, another partial double-layer gridshell (Gridshell-2) is generated.

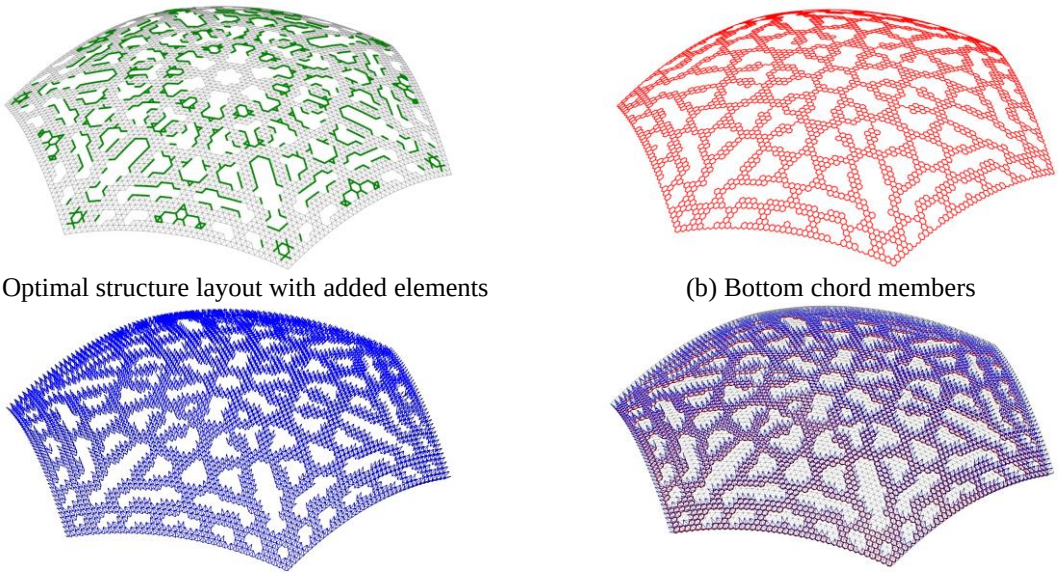

(a) Optimal structure layout with added elements (b) Bottom chord members

(c) Web-members (d) Gridshell-1

Figure 7: Illustration of the formation of partial double-layer gridshell

Linear static analysis is carried out to investigate the mechanical performance of the obtained partial double-layer gridshells (Gridshell-1&2). The dimensions of the gridshells are assumed to have a length unit of meter, i.e., its support-to-support distance is 60m and height is 20m. The structural members are assigned with a hollow circular section with outer diameter 150mm and wall thickness 5mm. The elasticity modulus of material is 2×10^{11}Pa, Poisson's ratio is 0.3. Same pattern of load as considered during the topology optimisation process is applied on the top layer but with an amplitude of 1kN. The deformation contours of these two structures under the external load are shown in Figure 8. For these two gridshells, the deformation is rather uniform among the whole structural domain, except for two regions, i.e., the support areas and the mid-span areas between two neighbouring supports, which exhibit the minimum and maximum deformation, respectively. In terms of the stress distribution, most of the elements are with small stress values, except for those locating in the support areas, as they need to gather the loads acting on the whole structures and transfer them to the supports. For simplicity, stress contours are not attached here. Note that, the linear static analysis carried out here can only reflect the mechanical properties of the gridshells in a very limited aspect. To demonstrate the advantages of the obtained partial double-layer gridshells over the single-layer structures or the fully double-layer gridshells, further comparative study is still needed.

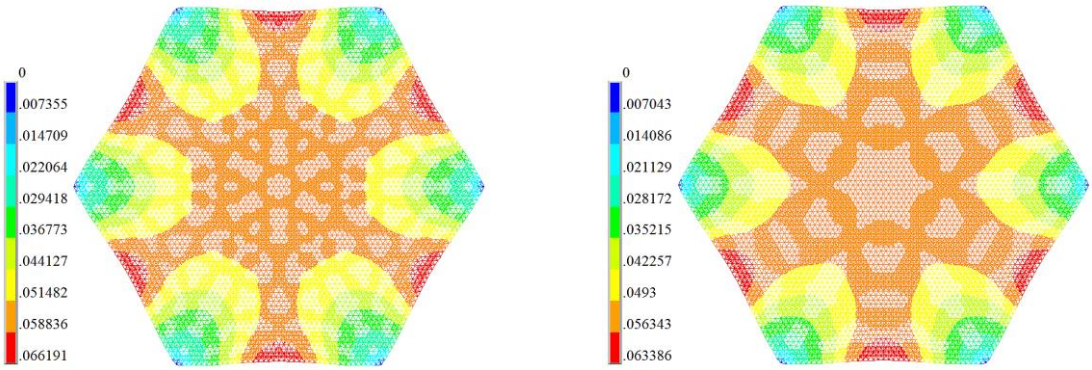

(a) Gridshell-1 (b) Gridshell-2

Figure 8: Deformation contours of the partial double-layer gridshells

5. Conclusion

This paper presents a discrete topology optimisation method which can simultaneously impose minimum and maximum feature size control on the solid phase in the structural layout. The method is tested on two examples, a planar cantilever beam and a hexagonal gridshell. The numerical results show that the proposed method can easily achieve the minimum and maximum feature size control of the solid phase. The method is applicable to planar and curved structures, and also capable of finding the optimal structural layouts under distributed load in addition to single concentrated force. The optimisation results of the single-layer hexagonal gridshell are used to guide the design of partial double-layer gridshells. Linear static analysis is carried out which shows the uniform stress and deformation distributions of the structures under the external loads. However, further study is still needed to reveal the possible mechanical advantages of the partial double-layer gridshells over the single-layer or fully double-layer structures.

Acknowledgements

The first author receives support from Chinese Scholarship Council (CSC) through the CSC-University of Bath Joint Scholarship. The share of MMA code from Prof. Krister Svanberg is also gratefully acknowledged.

References

[1] Andreassen, E., Anders C., Mattias S., Boyan S. and Sigmund O. Efficient Topology Optimization in MATLAB Using 88 Lines of Code. *Structural and Multidisciplinary Optimization*. 2011;43(1);1-16.
[2] Bourdin B., Filters in Topology Optimization. *International Journal for Numerical Methods in Engineering*, 2001; 50 (9); 2143–58.
[3] Chen, W., He Y., Fu G., Gong J. and Dong S. Stability Analysis of the Partial Double-Layer Forms Derived from the Complete Double-Layer Reticulated Dome. *Journal of the International Association for Shell and Spatial Structures*. 2001; 42 (137); 117–27.
[4] Dorn W., Gomory R. and Greenberg H. Automatic Design of Optimal Structures. *J. de Mecanique*. 1964; 3 (1): 25–52.
[5] Fairclough H., and Gilbert M. Layout Optimization of Simplified Trusses Using Mixed Integer Linear Programming with Runtime Generation of Constraints. *Structural and Multidisciplinary Optimization.* 2020; 61 (5); 1977–99.
[6] Fernández E., Collet M., Alarcón P., Bauduin S. and Duysinx P. An Aggregation Strategy of Maximum Size Constraints in Density-Based Topology Optimization. *Structural and Multidisciplinary Optimization.* 2019; 60 (5); 2113–30.
[7] Fernández E., Yang K., Koppen S. Alarcón P, Bauduin S. and Duysinx P. Imposing Minimum and Maximum Member Size, Minimum Cavity Size, and Minimum Separation Distance between Solid Members in Topology Optimization. *Computer Methods in Applied Mechanics and Engineering*. 2020;368.
[8] Guest, J., Prévost J. and Belytschko T. Achieving Minimum Length Scale in Topology Optimization Using Nodal Design Variables and Projection Functions. *International Journal for Numerical Methods in Engineering*. 2004.
[9] Guest J. Imposing Maximum Length Scale in Topology Optimization. *Structural and Multidisciplinary Optimization.* 2009; 37 (5); 463–73.
[10] He L., and Gilbert M. Rationalization of Trusses Generated via Layout Optimization. *Structural and Multidisciplinary Optimization*. 2015;52 (4); 677–94.
[11] Kanno Y. and Fujita S. Alternating Direction Method of Multipliers for Truss Topology Optimization with Limited Number of Nodes: A Cardinality-Constrained Second-Order Cone Programming Approach. *Optimization and Engineering*. 2017;327–58.
[12] Li L., Xie Z., Guo Y. and Liu F. Structural Optimization and Dynamic Analysis for Double-Layer Spherical Reticulated Shell Structures. *Journal of Constructional Steel Research.* 2006
[13] Parkes E. Joints in Optimum Frameworks. *International Journal of Solids and Structures*. 1975; 11 (9); 1017–22.
[14] Ramos A., and Paulino G. Filtering Structures out of Ground Structures – a Discrete Filtering Tool for Structural Design Optimization. *Structural and Multidisciplinary Optimization*. 2016; 54 (1); 95–116.
[15] Sigmund O. A 99 Line Topology Optimization Code Written in Matlab. *Structural and Multidisciplinary Optimization.* 2001; 21 (2); 120–27.
[16] sigmund O. Design of Material Structures Using Topology Optimization. Department of Solid Mechanics, 1994.
[17] Sigmund O. Morphology-Based Black and White Filters for Topology Optimization. *Structural and Multidisciplinary Optimization* 2007;33 (4–5); 401–24.
[18] Sigmund O. Manufacturing Tolerant Topology Optimization. *Acta Mechanica Sinica* 2009; 25 (2); 227–39.
[19] Svanberg K. The Method of Moving Asymptotes—a New Method for Structural Optimization. *International Journal for Numerical Methods in Engineering*. 1987.
[20] Tian L., Bai C., and Zhong W. Experimental Study and Numerical Simulation of Partial Double-Layer Latticed Domes against Progressive Collapse in Member-Removal Scenarios. *Structures*. 2021;29; 79–91.

[21] Wang F., Lazarov B. and Sigmund O. On Projection Methods, Convergence and Robust Formulations in Topology Optimization. *Structural and Multidisciplinary Optimization*. 2011; 43 (6); 767–84.
[22] Conway J., Burgiel, H. and Goodman-Strauss, C. The symmetries of things. *CRC Press*. 2016.